Mod Pathol 38 (2025) 100717

MODERN PATHOLOGY

USCAP UNITED STATES AND CANADIAN ACADEMY OF PATHOLOGY
Creating a Better Pathologist

Journal homepage: https://modernpathology.org/

Research Article

Classification of Fibro-Osseous Tumors in the Craniofacial Bones Using DNA Methylation and Copy Number Alterations

Tony G. Kleijn[a], Baptiste Ameline[b], Willem H. Schreuder[c,d,e], Károly Szuhai[f], Wierd Kooistra[a], Léon van Kempen[a,g], Ghazaleh S.H. Japalagh[a], Inge H. Briaire-de Bruijn[h], Stijn W. van der Meeren[i], Maarten C. Kleijwegt[j], Max Witjes[k], Sarina E.C. Pichardo[k], Wouter R. van Furth[l], Tereza Lausová[m], Gerben E. Breimer[n], Weibel Braunius[o], Jan de Lange[c,d], Kirsten van Langevelde[p], Herman M. Kroon[p], Mari F.C.M. van den Hout[q], Sjors A. Koppes[r], Simon Haefliger[b], Marc L. Ooft[s], Ilse C.H. van Engen-van Grunsven[t], Uta E. Flucke[t], Laura Hiemcke-Jiwa[n,u], Dilara C. Savci-Heijink[v], Gilles F.H. Diercks[a], Jan J. Doff[a], Albert J.H. Suurmeijer[a], Judith V.M.G. Bovée[h], Andreas von Deimling[m], Daniel Baumhoer[b,w], Arjen H.G. Cleven[a,v,*]

[a] *Department of Pathology and Medical Biology, University Medical Center Groningen, Groningen, the Netherlands;* [b] *Bone Tumor Reference Centre at the Institute for Medical Genetics and Pathology, University Hospital Basel, University of Basel, Basel, Switzerland;* [c] *Department of Oral and Maxillofacial Surgery, Amsterdam University Medical Centers, Amsterdam, the Netherlands;* [d] *Department of Oral Diseases and Maxillofacial Surgery, Academic Center for Dentistry Amsterdam (ACTA), Amsterdam, the Netherlands;* [e] *Department of Head and Neck Surgery and Oncology, Antoni van Leeuwenhoek, Amsterdam, the Netherlands;* [f] *Department of Cell and Chemical Biology, Leiden University Medical Center, Leiden, the Netherlands;* [g] *Department of Pathology, Antwerp University Hospital, University of Antwerp, Edegem, Belgium;* [h] *Department of Pathology, Leiden University Medical Center, Leiden, the Netherlands;* [i] *Department of Ophthalmology, Leiden University Medical Center, Leiden, the Netherlands;* [j] *Department of Head and Neck Surgery, Leiden University Medical Center, Leiden, the Netherlands;* [k] *Department of Oral and Maxillofacial Surgery/Head and Neck Surgery, University Medical Center Groningen, the Netherlands;* [l] *Department of Neurosurgery, Leiden University Medical Center, Leiden, the Netherlands;* [m] *Department of Neuropathology, Heidelberg University Medical Center, and CCU Neuropathology, German Cancer Center, DKFZ, Heidelberg, Germany;* [n] *Department of Pathology, University Medical Center Utrecht, Utrecht, the Netherlands;* [o] *Department of Head and Neck Surgical Oncology, University Medical Center Utrecht, Utrecht, the Netherlands;* [p] *Department of Radiology, Leiden University Medical Center, Leiden, the Netherlands;* [q] *Department of Pathology, GROW-School for Oncology and Reproduction, Maastricht University Medical Center, Maastricht, the Netherlands;* [r] *Department of Pathology, Erasmus University Medical Center, Rotterdam, the Netherlands;* [s] *Pathology-DNA, Rijnstate Hospital, Arnhem, the Netherlands;* [t] *Department of Pathology, Radboud University Medical Center, Nijmegen, the Netherlands;* [u] *Department of Pathology, Princess Máxima Center for Pediatric Oncology, Utrecht, the Netherlands;* [v] *Department of Pathology, Amsterdam University Medical Center, Amsterdam, the Netherlands;* [w] *Basel Research Centre for Child Health, Basel, Switzerland*

ARTICLE INFO

Article history:
Received 24 July 2024
Revised 9 December 2024
Accepted 13 January 2025
Available online 23 January 2025

Keywords:
copy number alterations
craniofacial bones

ABSTRACT

Fibro-osseous tumors of the craniofacial bones are a heterogeneous group of lesions comprising cemento-osseous dysplasia (COD), cemento-ossifying fibroma (COF), juvenile trabecular ossifying fibroma (JTOF), psammomatoid ossifying fibroma (PsOF), fibrous dysplasia (FD), and low-grade osteosarcoma (LGOS) with overlapping clinicopathological features. However, their clinical behavior and treatment differ significantly, underlining the need for accurate diagnosis. Molecular diagnostic markers exist for subsets of these tumors, including *GNAS* mutations in FD, *SATB2* fusions in PsOF, mutations involving the RAS-MAPK signaling pathway in COD, and *MDM2* amplification in LGOS. Because DNA methylation and copy number profiling are well established for the classification of central nervous system tumors, we aimed to investigate whether this tool might be used as well

These authors contributed equally to this work: Tony G. Kleijn, Baptiste Ameline, Daniel Baumhoer, and Arjen H.G. Cleven

* Corresponding author.
E-mail address: a.h.g.cleven@umcg.nl (A.H.G. Cleven).

https://doi.org/10.1016/j.modpat.2025.100717

DNA methylation
fibro-osseous tumor
osteosarcoma
profiling

for classifying fibro-osseous tumors in the craniofacial bones. We collected a well-characterized, multicenter cohort with available molecular data, including COD ($n = 20$), COF ($n = 13$), JTOF ($n = 10$), PsOF ($n = 25$), FD ($n = 23$), LGOS ($n = 4$), and high-grade osteosarcoma (HGOS; $n = 11$). Genome-wide DNA methylation and copy number variation data were generated using the Illumina Infinium Methylation EPIC array interrogating >850 000 CpG sites. DNA methylation profiling yielded evaluable results in 73/106 tumors, including 6 CODs, 12 COFs, 6 JTOFs, 19 PsOFs, 18 FDs, 2 LGOSs, and 10 HGOSs. Unsupervised clustering and dimensionality reduction (Uniform Manifold Approximation and Projection) revealed that FD, extragnatic PsOF, and HGOS formed distinct clusters. Surprisingly, COD, COF, JTOF, and mandibular PsOF clustered together, apart from other craniofacial bone tumors. LGOS did not form a distinct cluster, likely due to the low number of cases. Copy number analysis revealed that FD, COD, COF, JTOF, and PsOF were typically characterized by flat copy number profiles compared with LGOS with gains of chromosome 12 and HGOS with multiple heterogeneous copy number alterations. In conclusion, using DNA methylation and copy number profiles, benign fibro-osseous tumors can be separated from low-grade and HGOSs in the craniofacial bones, which is of diagnostic value in challenging cases with overlapping clinicopathological features.

Introduction

Fibro-osseous tumors of the craniofacial bones are rare and compromise a heterogeneous group of lesions, including cemento-osseous dysplasia (COD), cemento-ossifying fibroma (COF), juvenile trabecular ossifying fibroma (JTOF), psammomatoid ossifying fibroma (PsOF), fibrous dysplasia (FD), and low-grade central osteosarcoma (LGOS). Depending on clinical and radiographic features, COD can be divided into periapical, focal, florid, and familial florid subtypes that share an identical histomorphology.[1] Apart from FD and OS, which can arise in any bone, the other fibro-osseous lesions are predisposed to develop in the craniofacial bones, with COF restricted to the tooth-bearing areas of the jaws.[2]

Diagnosing fibro-osseous lesions can be difficult in routine clinical practice due to overlapping clinical, radiologic, and histopathological features. In addition, immunohistochemistry is generally not helpful in this regard. Although most fibro-osseous tumors are benign, accurate diagnosis is important as the treatment and outcome differ significantly between entities. For example, COD is usually asymptomatic and follows a self-limited course without requiring any intervention. Conversely, JTOF and PsOF need to be excised due to their continuous growth and expansion, which can result in facial disfigurement, impaired visual function, and sinus dysfunction.[3] FD often stabilizes when the patient reaches skeletal maturity; therefore, it is generally recommended to wait until the lesion becomes quiescent and the patient has reached skeletal maturity before performing an operation.[4] In contrast, low-grade OS necessitates resection without delay to prevent metastasis.[5]

In recent years, significant progress has been made in the molecular understanding of fibro-osseous tumors.[3] Although clinical and radiologic correlation with morphologic features remains the cornerstone for diagnosis, identifying specific genetic abnormalities can be helpful in diagnostic decision making. For example, molecular assays can confirm FD, which is caused by activating *GNAS* mutations at codon 201, most commonly p.(Arg201His) or p.(Arg201Cys), resulting in the constitutive activation of Wnt/β-catenin signaling pathway.[6] In a recent study by Haefliger et al,[7] pathogenic hotspot mutations in *BRAF*, *HRAS*, *KRAS*, *NRAS*, and *FGFR3* were identified in 5/18 cases of COD, suggesting that COD might be at least partly driven by RAS-MAPK activation. We previously reported that *SATB2* rearrangement is a recurrent molecular alteration specific to PsOF, leading to a truncated protein lacking key functional domains.[8] Molecular findings from various studies indicate that COFs are heterogeneous, and the exact molecular mechanisms underlying their pathogenesis remain unclear.[9-11] In patients with autosomal dominant hyperparathyrodism-jaw tumor (HPT-JT) syndrome, however, *CDC73* (*HRPT2*) mutations were detected. *CDC73* is a tumor suppressor gene encoding the parafibromin protein, a transcriptional and post-transcriptional regulator that targets both the Wnt/β-catenin and Hedgehog pathways. In the pathogenesis of sporadic COF, *CDC73* loss-of-function mutations seem to play only a minor role as the reported frequency was only 5%.[12]

Distinguishing LGOS from other fibro-osseous lesions can be difficult. Approximately 30% of LGOSs harbor amplification of *MDM2*, which can be confirmed using fluorescence in situ hybridization (FISH).[5,13,14] In contrast to LGOS, high-grade osteosarcomas (HGOSs) have complex karyotypes, featuring abundant structural and numeric aberrations, often resulting from chromothripsis.[15]

Given the recent implementation of DNA methylation-based classification in central nervous system tumors and its emerging role for bone and soft tissue tumor classification,[16,17] this study aimed to investigate whether DNA methylation and copy number profiling can be used as an additional diagnostic tool to improve diagnostic accuracy in fibro-osseous tumors of the craniofacial bones.

Materials and Methods

Patient Samples

Tumor tissues were obtained from the archives of the pathology departments of the Amsterdam University Medical Center, Erasmus University Medical Center, Leiden University Medical Center, Maastricht University Medical Center, Radboud University Medical Center, University Medical Center Groningen, and University Medical Center Utrecht in the Netherlands, and from the Institute of Pathology at the University Hospital Basel in Switzerland. Diagnoses were based on standard histopathological criteria in conjunction with clinical and radiologic features

according to the current 2024 WHO classification.[1] These features are described in great detail in our reviews.[3,5] In total, 106 fibro-osseous tumors from 104 patients from 2000 to 2023 were retrieved with available formalin-fixed paraffin-embedded (FFPE) or fresh frozen tumor tissue from biopsy or resection material that was preferably not decalcified with formic acid. All available material and ancillary techniques performed during the initial diagnostic workup were reviewed, including hematoxylin and eosin staining, immunohistochemistry, and molecular assays. This was performed by expert bone and soft tissue tumor pathologists (A.C. and D.B.) to confirm the diagnosis. We included COD ($n = 20$), COF ($n = 13$), JTOF ($n = 10$), PsOF ($n = 25$), FD ($n = 23$), LGOS ($n = 4$), and HGOS ($n = 11$) in our study series.

Samples were retrieved from the bone and soft tissue tumor archives as approved by the ethical board (UMCG: RR202200287; LUMC: B21.022), and coded (pseudonymized) according to the Dutch Code Proper Secondary Use of Human Tissue according to the Dutch Society of Pathology (Federa). Research use of tissues and anonymization of data were in accordance with local ethical approvals.

DNA Extraction

Genomic DNA was extracted from FFPE and fresh frozen tumor tissue using only representative tissue with a tumor content of at least 60%. DNA extraction from FFPE tissue was performed using the QIAamp DNA FFPE Tissue Kit (QIAGEN,) according to the manufacturer's instructions, and from fresh frozen tissue using a salt/chloroform-based protocol. The DNA was quantified using a Qubit Fluorometer. Tumors from which more than 100 ng genomic DNA could be extracted were selected for array-based DNA methylation analysis. Twenty-one FFPE samples were excluded owing to limited genomic DNA availability, leaving 85 samples for analysis.

DNA Methylation Data Sets

Genome-wide methylation data were generated from 85 cases using the Illumina Infinium Human MethylationEPIC v1.0 BeadChip or its successor v2.0 BeadChip (EPICv2), which covered 850,000 and 935,000 CpG sites across the genome, respectively. DNA derived from FFPE samples was restored using the Illumina FFPE DNA Restoration Kit according to the manufacturer's instructions. Sixty-one FFPE and 12 fresh frozen samples yielded interpretable results, whereas 12 FFPE samples failed to meet quality control standards owing to insufficient tissue preservation.

In total, 73/106 included tumors yielded evaluable DNA methylation data, including 6 CODs, 12 COFs, 6 JTOFs, 19 PsOFs, 18 FDs, 2 LGOSs, and 10 HGOSs. The raw methylation data were processed together with published external data sets, including FD ($n = 18$), HGOS ($n = 68$), ameloblastoma ($n = 5$), aneurysmal bone cyst ($n = 32$), giant cell granuloma ($n = 12$), osteoblastoma ($n = 37$), and odontogenic myxoma ($n = 10$).[18-27] The tumor locations of the external FDs, HGOSs, aneurysmal bone cysts, and osteoblastomas were partially outside of the craniofacial bones. Sample details are provided in Supplemental Table S1.

Methylation Array Processing

Raw intensity data files from the MethylationEpic BeadChips were processed using the R-package "minfi" (https://bioconductor.org/packages/minfi/). The "convertArray" function from "minfi" was manually edited to convert EPICv2 arrays into a virtual EPICv1 array for joint normalization and data processing from both platforms. Probes associated with known single-nucleotide polymorphisms, non-CpG islands, and sex chromosomes were excluded from the analysis. Additionally, samples with a mean detection P value of >.03 were removed. The "preprocessQuantile" function was employed before generating dimension reduction visualization, whereas the "preprocessIllumina" function was used before deriving copy number profiles. Finally, batch effect corrections were applied to the beta values using the R-package "ChAMP" (https://bioconductor.org/packages/ChAMP/) to eliminate any bias related to the sample type (FFPE/fresh frozen) and the array type (450K/EPICv1/EPICv2).

Unsupervised Clustering

The list of probes was subsequently narrowed down to the top 25,000 most differentially methylated CpG sites. An unsupervised nonlinear dimension reduction method, Uniform Manifold Approximation and Projection, was performed on the results of a principal component analysis (PCA) calculated via the singular value decomposition of the beta methylation matrix. A graph was generated using the R-package "uwot" (https://github.com/jlmelville/uwot). The settings used to generate the nonlinear regression model were PCA = 40, neighbors = 8, and the remaining parameters were left unchanged. The selection of the number of PCA fulfilled 2 criteria: (1) explained variance greater than 70%, and (2) the reference samples used as positive controls were displayed in their expected clusters.

Copy Number Variation Analysis

Copy number profiles were derived from the methylation array data using the R-package "conumee" (http://bioconductor.org/packages/conumee/), following the preprocessing of data as described above. The default settings of conumee were used for copy number segmentation[28] and were as follows: a minimum of 25 probes per bin and a minimum bin size of 50,000 bp. Copy number variations were considered significant if at least 5 adjacent bins exceeded the threshold value. Each copy number profile was reviewed individually.

Results

Clinicopathological Characteristics of Fibro-osseous Bone Tumors

The median age at diagnosis of each patient group varied in our series as follows: COD, 40 years (range, 20-51); COF, 37 years (range, 11-55); JTOF, 12 years (range, 4-29); PsOF, 20 years (range, 9-41); FD, 44 years (range, 12-71); LGOS, 26.5 years (range, 11-43); and HGOS, 67 years (range, 30-76). The male/female ratios were 1:9, 8:5, 7:3, 16:9, 12:7, 4:0, and 6:5, respectively. COD lesions were of periapical ($n = 11$), focal ($n = 5$), and florid ($n = 4$) subtypes. The mandible was the most commonly affected jawbone for COD (18/20), COF (11/13), and JTOF (5/10), whereas PsOF primarily occurred in the extragnathic bones (19/25). LGOSs were located in the maxilla ($n = 2$) and mandible ($n = 2$). FDs and HGOSs were located in several craniofacial bones and the skull. Clinical information and available genetic data are summarized in the Table.[3,7,8]

Table
Clinicopathological characteristics of study cases

Study ID	Age (years)	Sex	Location	Genetics	Array	Reference
COD_1[P]	44	Female	Maxilla	WT[a]	EPIC v1.0	
COD_2[P]	33	Female	Mandible	NP	EPIC v1.0	
COD_3[P]	39	Female	Mandible	WT[a]	EPIC v2.0	
COD_4[P]	44	Male	Mandible	WT[a]	EPIC v2.0	
COD_5[P]	46	Female	Mandible	WT[a]	Failed[c]	
COD_6[P]	42	Female	Mandible	WT[b]	EPIC v2.0	Haefliger et al[7]
COD_7[Fo]	43	Female	Mandible	WT[b]	EPIC v2.0	Haefliger et al[7]
COD_8[Fo]	20	Female	Mandible	WT[b]	Failed[d]	Haefliger et al[7]
COD_9[P]	42	Female	Mandible	WT[b]	Failed[d]	Haefliger et al[7]
COD_10[Fl]	35	Female	Mandible	*HRAS* mut	Failed[d]	Haefliger et al[7]
COD_11[Fo]	51	Female	Mandible	*FGFR3* mut	Failed[d]	Haefliger et al[7]
COD_12[P]	39	Female	Mandible	WT[b]	Failed[d]	Haefliger et al[7]
COD_13[P]	29	Female	Mandible	WT[b]	Failed[d]	Haefliger et al[7]
COD_14[P]	48	Male	Mandible	WT[b]	Failed[d]	Haefliger et al[7]
COD_15[Fl]	29	Female	Mandible	WT[b]	Failed[d]	Haefliger et al[7]
COD_16[Fl]	31	Female	Mandible	WT[b]	Failed[d]	Haefliger et al[7]
COD_17[Fo]	41	Female	Mandible	*NRAS* mut	Failed[d]	Haefliger et al[7]
COD_18[Fl]	33	Female	Mandible	*KRAS* mut	Failed[d]	Haefliger et al[7]
COD_19[P]	28	Female	Maxilla	WT[b]	Failed[d]	Haefliger et al[7]
COD_20[Fo]	46	Female	Mandible	*BRAF* mut	Failed[d]	Haefliger et al[7]
COF_1	46	Male	Mandible	WT for *GNAS*	EPIC v1.0	
COF_2	55	Male	Mandible	NP	Failed[d]	
COF_3	11	Male	Mandible	WT for *GNAS*	EPIC v1.0	
COF_4	16	Female	Mandible	NP	EPIC v1.0	
COF_5	25	Female	Maxilla	NP	EPIC v1.0	
COF_6	27	Male	Maxilla	NP	EPIC v1.0	
COF_7	37	Male	Mandible	NP	EPIC v1.0	
COF_8	54	Female	Mandible	NP	EPIC v1.0	
COF_9	37	Male	Mandible	NP	EPIC v1.0	
COF_10	27	Male	Mandible	NP	EPIC v2.0	
COF_11	43	Female	Mandible	NP	EPIC v2.0	
COF_12	38	Female	Mandible	NP	EPIC v1.0	
COF_13	55	Male	Mandible	NP	EPIC v1.0	
FD_1	NA	NA	Jaw	*GNAS* mut	Failed[c]	
FD_2	NA	NA	Jaw	*GNAS* mut	Failed[c]	
FD_3	25	Male	Maxilla	*GNAS* mut	EPIC v1.0	
FD_4	44	Female	Zygoma	*GNAS* mut	EPIC v1.0	
FD_5	32	Male	Concha	NP	EPIC v1.0	
FD_6	22	Female	Mastoid	*GNAS* mut	EPIC v1.0	
FD_7	12	Male	Skull	*GNAS* mut	EPIC v1.0	
FD_8	47	Male	Sinus frontalis/ethmoidalis	*GNAS* mut	Failed[c]	
FD_9	27	Male	Sinus sphenoidalis	*GNAS* mut	EPIC v1.0	
FD_10	54	Female	Sinus maxillaris/zygoma	*GNAS* mut	EPIC v1.0	
FD_11	42	Female	Mastoid	*GNAS* mut	Failed[d]	
FD_12	45	Male	Skull	*GNAS* mut	EPIC v1.0	
FD_13	56	Male	Retroauricular	*GNAS* mut	EPIC v1.0	
FD_14	57	Male	Mastoid	*GNAS* mut	EPIC v1.0	
FD_15	16	Female	Frontal bone	*GNAS* mut	EPIC v1.0	
FD_16	40	Female	Skull (parietal/frontal)	*GNAS* mut	EPIC v1.0	
FD_17	71	Male	Epitympanum	*GNAS* mut	EPIC v1.0	
FD_18[e]	44	Female	Skull	*GNAS* mut	EPIC v1.0	
FD_19[e]	44	Female	Posterior cranial fossa	*GNAS* mut	EPIC v1.0	
FD_20[e]	44	Female	Posterior cranial fossa	*GNAS* mut	EPIC v1.0	
FD_21	29	Male	Mandible	WT for *GNAS*	EPIC v1.0	
FD_22	44	Male	Sinus sphenoidalis	*GNAS* mut	Failed[d]	
FD_23	45	Male	Sinus maxillaris	*GNAS* mut	EPIC v2.0	
JTOF_1	4	Male	Maxilla	*SATB2* FISH no split	Failed[c]	Cleven et al[8]
JTOF_2	12	Male	Mandible	*SATB2* FISH no split	Failed[c]	Cleven et al[8]
JTOF_3	12	Female	Mandible	*SATB2* FISH no split	EPIC v1.0	Cleven et al[8]
JTOF_4	23	Male	Maxilla	*SATB2* FISH no split	Failed[c]	Cleven et al[8]
JTOF_5	4	Male	Sinus maxillaris	*SATB2* FISH no split	EPIC v1.0	Cleven et al[8]
JTOF_6	29	Male	Mandible	*SATB2* FISH no split	EPIC v1.0	Cleven et al[8]
JTOF_7	13	Male	Mandible	NP	Failed[c]	

Table (*continued*)

Study ID	Age (years)	Sex	Location	Genetics	Array	Reference
JTOF_8	25	Female	Maxilla	NP	EPIC v2.0	
JTOF_9	7	Male	Maxilla	NP	EPIC v2.0	
JTOF_10	10	Female	Mandible	NP	EPIC v2.0	
PsOF_1	41	Female	Orbita	*SATB2* FISH no split	Failed[d]	Cleven et al[8]
PsOF_2	25	Male	Sinus maxillaris	*SATB2* FISH no split	EPIC v1.0	Cleven et al[8]
PsOF_3	10	Male	Nose	*SATB2* FISH no split	EPIC v1.0	Cleven et al[8]
PsOF_4	26	Male	Mandible	*SATB2* FISH no split	EPIC v1.0	Cleven et al[8]
PsOF_5	12	Female	Orbita	*SATB2* FISH split	EPIC v1.0	Cleven et al[8]
PsOF_6	11	Male	Orbita	*SATB2* FISH split	EPIC v1.0	Cleven et al[8]
PsOF_7	34	Male	Mandible	*SATB2* FISH split	EPIC v1.0	Cleven et al[8]
PsOF_8	9	Female	Mandible	*SATB2* FISH split	EPIC v1.0	Cleven et al[8]
PsOF_9	39	Male	Sinus maxillaris	Failed	Failed[c]	Cleven et al[8]
PsOF_10	12	Male	Orbita	*SATB2* FISH split	EPIC v1.0	Cleven et al[8]
PsOF_11	14	Male	Mandible	*SATB2::AL513487.1* fusion	EPIC v1.0	
PsOF_12	24	Female	Sphenoid bone	NP	EPIC v1.0	
PsOF_13	20	Female	Ethmoid bone	NP	Failed[c]	
PsOF_14	20	Male	Sinus sfenoidalis	NP	EPIC v1.0	
PsOF_15	16	Male	Mandible	NP	Failed[d]	
PsOF_16	23	Female	Ethmoid bone	NP	EPIC v1.0	
PsOF_17	11	Male	Clivus/sinus sphenoidalis	NP	EPIC v1.0	
PsOF_18	10	Male	Ethmoid bone	NP	Failed[c]	
PsOF_19	38	Male	Sinus frontalis	NP	Failed[d]	
PsOF_20	10	Male	Nasal cavity	NP	EPIC v1.0	
PsOF_21	26	Female	Orbita	NP	EPIC v2.0	
PsOF_22	10	Male	Sinus nasale	NP	EPIC v2.0	
PsOF_23	41	Female	Mandible	NP	EPIC v2.0	
PsOF_24	20	Male	Sinus sfenoidalis	NP	EPIC v2.0	
PsOF_25	9	Female	Maxilla	NP	EPIC v2.0	
LGOS_1	43	Male	Maxilla	*TP53* mut; *FGFR3* mut; IHC *MDM2* negative	EPIC v1.0	
LGOS_2	21	Male	Mandible	FISH *MDM2* negative	EPIC v2.0	
LGOS_3	11	Male	Maxilla	NA	Failed[d]	
LGOS_4	32	Male	Mandible	IHC *MDM2* negative	Failed[d]	
HGOS_1	66	Female	Mandible	NP	EPIC v1.0	
HGOS_2	73	Female	Mandible	NP	EPIC v1.0	
HGOS_3	30	Female	Skull (base)	NP	EPIC v1.0	
HGOS_4	62	Male	Concha	NP	EPIC v1.0	
HGOS_5	60	Male	Maxilla	NP	EPIC v1.0	
HGOS_6	44	Male	Maxilla	NP	EPIC v1.0	
HGOS_7	76	Female	Maxilla	NP	EPIC v1.0	
HGOS_8	67	Male	Maxilla	NP	EPIC v2.0	
HGOS_9	76	Male	Orbita	*MDM2* amplification	EPIC v2.0	
HGOS_10	73	Male	Sphenoid/rostrum	NP	Failed[c]	
HGOS_11	68	Female	Maxilla	NP	EPIC v2.0	

COD, cemento-osseous dysplasia; COF, cemento-ossifying fibroma; FD, fibrous dysplasia; JTOF, juvenile trabecular ossifying fibroma; HGOS, high-grade osteosarcoma; LGOS, low-grade osteosarcoma; mut, mutant; NA, not available; NP, not performed; PsOF, psammomatoid ossifying fibroma; WT, wildtype.
P, periapical. Fl, florid. Fo, focal.

[a] Wild type for mutations involved in RAS-MAPK pathway, including *BRAF, FGFR3, HRAS, KRAS,* and *NRAS.*
[b] Wildtype in Oncomine Focus DNA Panel (hotspots of 35 genes).
[c] DNA methylation data failed quality control.
[d] Too low DNA concentration for methylation array.
[e] Tumor tissue was derived from the same patient.

Representative radiologic and morphologic features of each tumor subtype are shown in Figures 1 and 2.

Microscopically, COFs were composed of a variable mixture of monomorphic fibroblastic spindle cells, immature bone trabeculae, and cementum-like material (Fig. 1B). Osteoblastic rimming was prominent, and the stroma varied in cellularity. No significant atypia was observed. Some COFs were surrounded by a thin layer of connective tissue, preventing fusion of lesional and preexisting bone. JTOFs were composed of fibrous stroma with spindled-to-stellate fibroblastic cells with bands of osteoid without osteoblastic rimming together with immature bony trabeculae surrounded by plump osteoblasts (Fig. 1D). The mineralized tissue appeared to develop directly from the stromal cells and appeared immature and woven in structure. PsOFs had characteristically small spherical ossicles of bone (psammomatoid bodies) rimmed with flattened osteoblasts (Fig. 1F). All COD cases had fibroblastic stroma with variable cellularity and a heterogeneous osseous component composed of woven bone and cementum-like material (Fig. 2B). FDs was composed of mature fibrous tissue with bland-appearing fibroblastic cells and immature woven bone formation, often with a peculiar curvilinear architecture (Fig. 2D). Typically, osteoblastic rimming was absent. Sharpey's fibers radiating perpendicularly from the immature matrix into the surrounding stroma was commonly observed. The lesional matrix

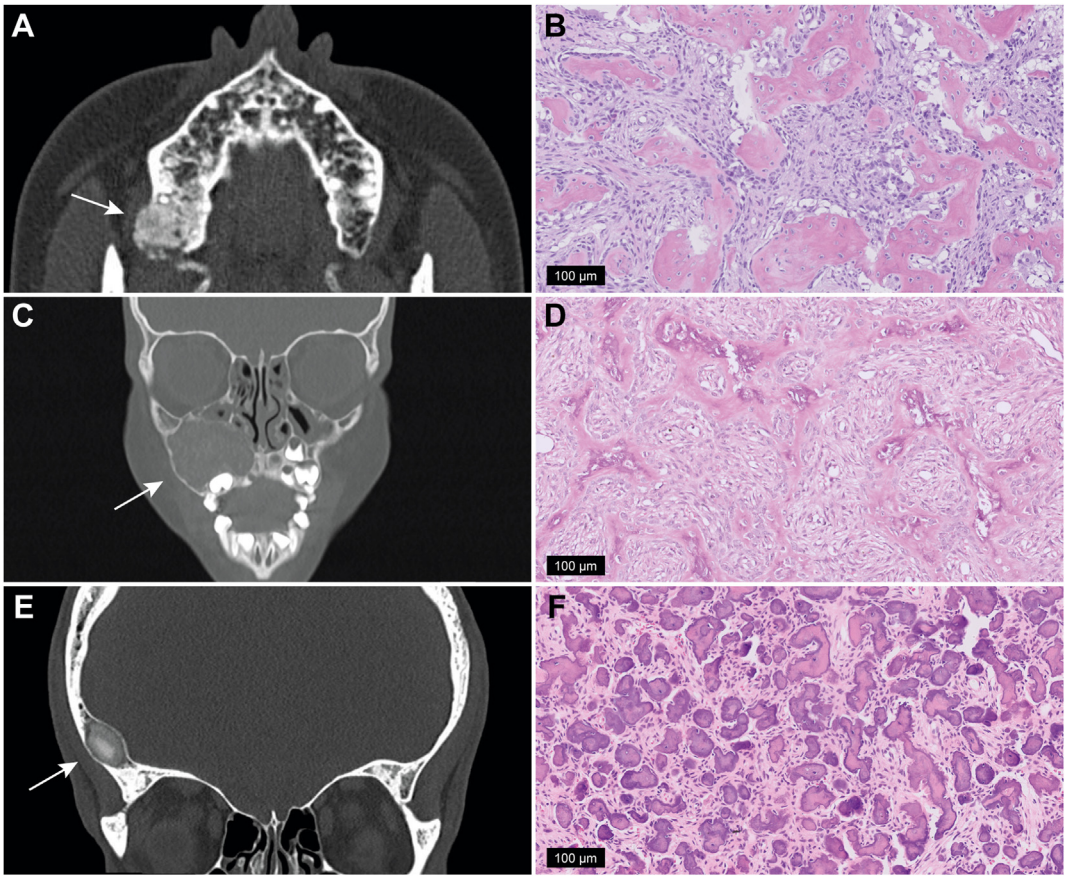

Figure 1.
Representative imaging and morphologic examples of craniofacial fibro-osseous tumors. (A) Axial computed tomography (CT) image of cemento-ossifying fibroma (COF_5) showed a sclerotic mass in the right maxilla. (B) COF_3 showed woven bone trabeculae with osteoblastic rimming within cellular fibroblastic stroma. (C) Coronal CT image of juvenile trabecular ossifying fibroma (JTOF_9) showed an expanding bone lesion in the right upper jaw with a heterogeneous appearance and several denser intralesional components. On the medial side, the lesion extended into the nasal cavity, compressing the inferior concha, and expanded superiorly into the maxillary sinus without signs of cortical destruction. (D) JTOF_8 showed cellular fibrous stroma composed of spindled-to-stellate fibroblastic cells with immature bony trabeculae surrounded by plump osteoblasts. (E) Coronal CT image of psammomatoid ossifying fibroma (PsOF_19) showed a well-defined lesion in the right frontal bone. (F) PsOF_6 with confirmed *SATB2* fusion showed a cellular bland spindle cell component and characteristic small spherical ossicles (psammomatoid bodies). The tumors are indicated by white arrows.

in FD was commonly fused to the adjacent normal bone. Low-grade central OSs showed minimal pleomorphism and subtle atypical fibroblastic cells with scarce mitotic activity and irregular trabeculae of woven bone (Fig. 2F).

Methylome Analysis and Uniform Manifold Approximation and Projection-Based Classification

In total, 73/106 included tumors yielded evaluable DNA methylation data, including 6 CODs, 12 COFs, 6 JTOFs, 19 PsOFs, 18 FDs, 2 LGOSs, and 10 HGOSs. In the COD group 14 of 20 cases failed; the 6 CODs with evaluable DNA methylation data were of the periapical subtype. All COFs were sporadic and not associated with HPT-JT syndrome. The 2 cases of LGOSs with interpretable methylation data were of the central subtype, and had no *MDM2* amplification (excluded by immunohistochemistry or FISH). LGOS case #1 had a pathogenic *TP53* and *FGFR3* mutation.

Unsupervised cluster analysis revealed that FD, extragnatic PsOF, and HGOS formed distinct clusters, whereas COD, COF, and JTOF clustered together, based on their DNA methylation profiles (Fig. 3). Within the FD cluster, separate clusters composed of FD in the craniofacial bones and skull versus FD located in the ribs or lower limbs were recognized. Interestingly, all PsOF cases located in the mandible ($n = 5$), 3 of which had confirmed *SATB2* rearrangements, did not cluster in the extragnatic PsOF group but clustered in the heterogeneous group of COD, COF, and JTOF. With regard to anatomical location, we did not observe clear separate clusters between HGOSs from the craniofacial bones/skull and those from other bones of the skeleton. The 2 LGOS cases did not cluster together, likely because of the low number of cases: 1 LGOS without *GNAS* mutation was positioned in the FD cluster, and the other clustered in the heterogeneous cluster composed of COD, COF, and JTOF. None of the benign fibro-osseous tumors of our study cohort clustered with tumors in the reference cohort, consisting of ameloblastomas, aneurysmal bone cysts, giant cell granulomas, odontogenic myxomas, and osteoblastomas.

Cases that did not cluster in their expected clusters were re-evaluated. None of the diagnoses required adjustment after re-evaluation. None of the non-FD cases that clustered incorrectly with the FDs harbored a *GNAS* mutation, and histologically, they exhibited no characteristics consistent with older FD with regressive changes, which frequently lack *GNAS* mutations.

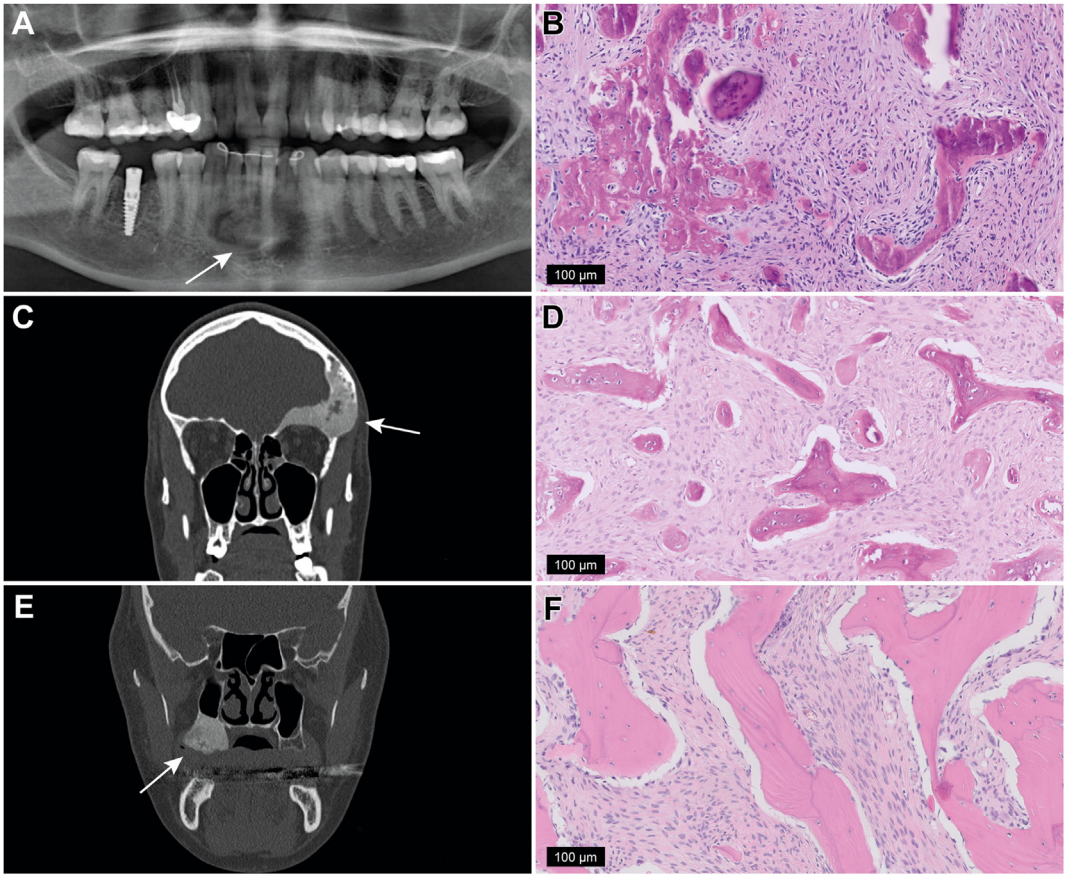

Figure 2.
Representative imaging and morphologic examples of craniofacial fibro-osseous tumors. (A) Orthopantomogram of cemento-osseous dysplasia (COD_3) demonstrated in the anterior mandible a central radiopaque mass surrounded by a radiolucent rim in the apical region of the lower incisors. (B) COD_3 showed various proportions of mineralized woven bone trabeculae embedded in moderately cellular and monomorphic fibroblastic stroma. (C) Coronal CT image of fibrous dysplasia (FD_15) showed an expansile lesion in the left frontal bone with a typical ground-glass appearance, without cortical interruption or soft tissue extension. (D) FD_14 with confirmed *GNAS* mutation showed woven bone deposition in a bland spindle cell proliferation background, and Sharpey's fibers radiate into the surrounding stroma. Prominent osteoblastic rimming was absent. (E) Coronal CT image of low-grade central osteosarcoma (LGOS_1) showed a sclerotic, expansile lesion in the right posterior maxilla, with involvement of the floor of the maxillary sinus. (F) LGOS_1 showed spindle cells with mild nuclear atypia between irregular lamellar bone. The tumors are indicated by white arrows. COD, Cemento-osseous dysplasia; CT, computed tomography; FD, fibrous dysplasia; LGOS, Low-grade osteosarcomas.

Copy Number Analysis

Copy number analysis revealed that COD (6/6), COF (12/12), PsOF (16/19), and FD (32/34) were typically characterized by flat copy number profiles compared with LGOS with gains of chromosome 12 (2/2; Fig. 4A) and HGOS with heavily rearranged genomes characterized by multiple heterogeneous copy number alterations (11/11; Fig. 4B). The LGOSs did not reveal high-level amplifications, particularly not *MDM2*, *CDK4*, *MDM4*, or *CDK6*.

Two FDs with confirmed *GNAS* mutations showed copy number alterations: FD case #7 showed a small deletion on chromosome 22, whereas FD case #16 showed multiple alterations including focal gains of chromosome 11 and toward the telomeric region of chromosome 15q (Supplementary Fig. S1). Three PsOFs showed copy number alterations: PsOF case #11 (*SATB2* FISH positive) harbored a small loss of chromosome 4, PsOF case #25 showed a focal gain of chromosome 6, and PsOF case #3 showed a gain of chromosome 12 without high-level *MDM2* amplification (immunohistochemistry and FISH confirmed the absence of *MDM2* amplification; Supplementary Fig. S2).

Copy number profiles of JTOFs were generally flat, with 2 of cases showing copy number alterations: JTOF case #5 had a focal loss of chromosome 6, and JTOF case #9 had losses of chromosomes 6 and 19 and a partial gain of chromosome 21 (Supplementary Fig. S3).

Discussion

Fibro-osseous tumors of the craniofacial bones are a heterogeneous group of lesions. Due to overlap in clinicopathological features, clear separation of benign craniofacial bone tumors from more aggressive or malignant subtypes can be difficult and challenging. In this study, we explored the diagnostic value of DNA methylation and copy number profiles in fibro-osseous tumors of the craniofacial bones.

Our data showed that FD, extragnatic PsOF, and HGOS showed distinct DNA methylation patterns, whereas COD, COF, JTOF, and mandibular PsOF clustered together. Copy number profiling differentiated low-grade and HGOSs from benign fibro-osseous tumors in the craniofacial bones.

Recently, the German Cancer Research Center's (DKFZ) sarcoma DNA methylation classifier was developed, covering 62 soft tissue and bone tumor entities,[18] which has been validated by

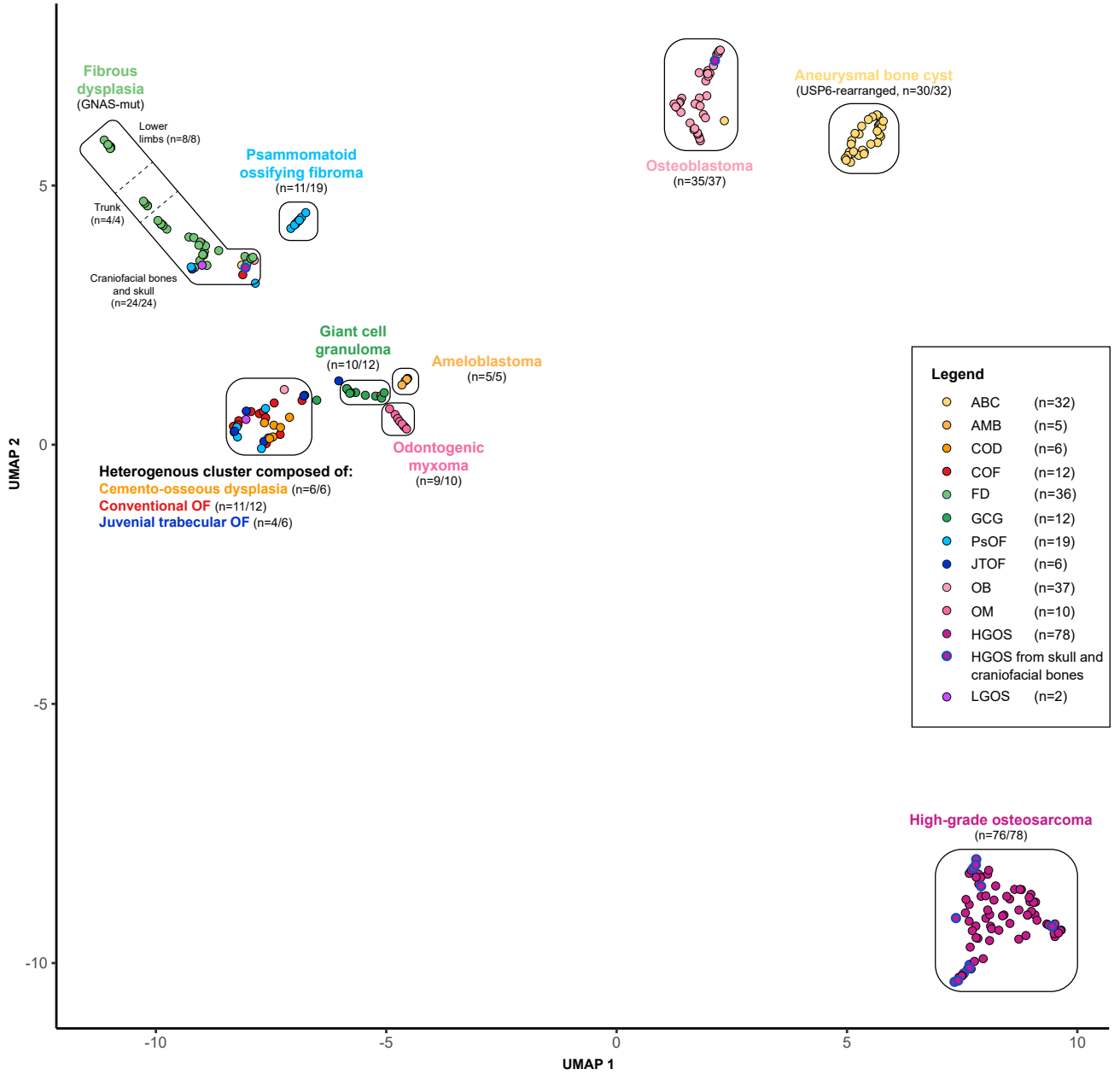

Figure 3.
Methylation-based clustering of craniofacial fibro-osseous tumors. Unsupervised cluster analysis revealed that fibrous dysplasia (FD), extragnatic PsOF, and HGOS formed distinct clusters. The clustering of FD was partially based on tumor location, with distinct clusters composed of FD from the craniofacial bones and skull, ribs, and lower limbs. HGOSs from the craniofacial bones and skull (encircled in blue) did not cluster differently than those from other bones of the skeleton. COD, COF, and JTOF formed a heterogeneous cluster. LGOSs did not form a distinct cluster and were positioned in the FD cluster and heterogeneous cluster composed of COD, COF, and JTOF. The benign fibro-osseous tumors did not cluster with AMB, ABC, GCG, OM, and OB. COD, Cemento-osseous dysplasia, COF, cemento-ossifying fibroma; ABC, aneurysmal bone cyst; AMB, ameloblastoma; GCG, giant cell granuloma; HGOS, high-grade osteosarcoma; JTOF, juvenile trabecular ossifying fibroma; LGOS, Low-grade osteosarcomas; PsOF, psammomatoid ossifying fibroma; OB, osteoblastoma; OM, odontogenic myxoma.

several groups with independent and well-characterized series of soft tissue and bone tumors.[19,29,30] The sensitivity and specificity of individual tumor classes vary, with fusion-driven neoplasms typically forming more distinct clusters, and molecular less well-defined lesions showing more ambiguous results.[31] In line with our results, HGOS and FD are tumor subtypes that are well recognized by this classifier based on DNA methylation patterns. A new finding in our study was the observation that clustering of FD was partially influenced by tumor localization, as FD originating from the head and neck region, ribs, and lower limbs formed separate clusters. The craniofacial bones have unique properties compared with other bones, which mainly result from their distinct embryonic development.[32] Because DNA methylation plays an important role in bone development and osteoclast differentiation, it is likely that the osteoprogenitor cells in the craniofacial bones from which FD arises have distinct DNA methylation patterns compared with those in other bones of the skeleton. Furthermore, tumor location-dependent differences in

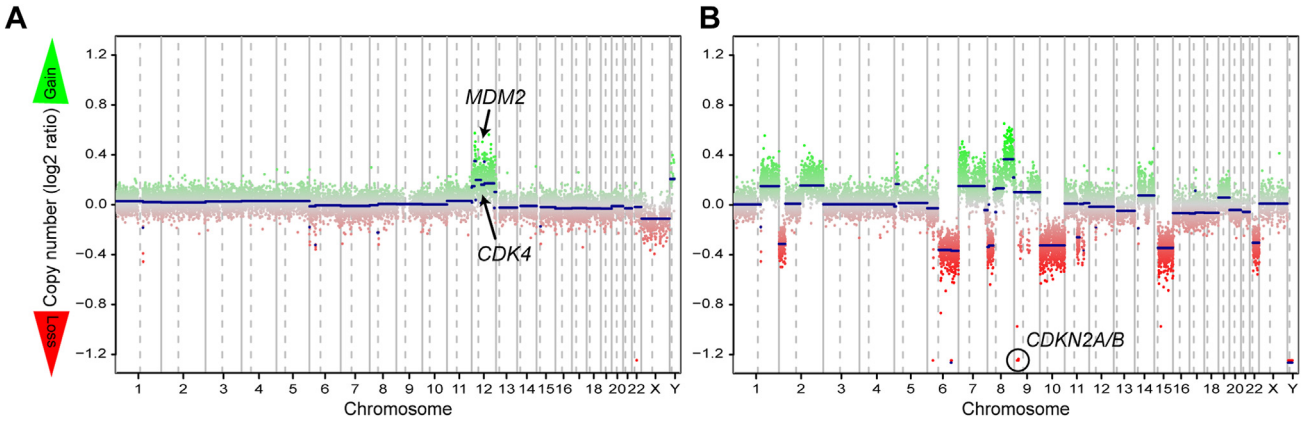

Figure 4.
Copy number profiles. (A) Low-grade osteosarcoma (LGOS_1) with a gain of chromosome 12, without high-level amplifications of *MDM2* and *CDK4*. (B) HGOS (HGOS_1) with multiple copy number alterations including homologous deletion of *CDKN2A/B*. HGOS, high-grade osteosarcoma; LGOS, Low-grade osteosarcomas.

DNA methylation together with tumor site-specific enrichment for specific chromosomal changes and genetic mutations has been described in other neoplasms as well.[33]

Regarding the DNA methylation findings in the other fibro-osseous tumor subtypes in the current study, such as extragnatic PsOF that formed a distinct methylation cluster, no external DNA methylation data of PsOF cases were available for comparison with our set. Nevertheless, our data confirm that PsOF is a molecular distinct subtype of the craniofacial fibro-osseous tumors with specific *SATB2* fusions, as well as a specific DNA methylation profile. Likewise with FD, PsOF appears to share DNA methylation profiles partly pending on the tumor location as mandibular and extragnatic PsOFs did not cluster together.

The co-clustering of COF, COD, and JTOF suggests that they are at least epigenetically part of the same spectrum, however, the clinical presentation and behavior are significantly different between these entities, varying from self-limiting growth in COD and locally aggressive growth in COF and JTOF. In line with the ambiguous results of the DKFZ sarcoma classifier in molecularly less well-defined lesions, our findings in COF, COD, and JTOF likely reflect the same methodologic problem caused by the lack of specific molecular markers to confirm the diagnosis and the smaller numbers of well-preserved tissue samples of COD and JTOF with interpretable DNA methylation results. Furthermore, tumor location appears to be a factor in the co-clustering, as all cases in the heterogenous cluster originate from the mandible or maxilla, including the 5 mandibular PsOFs. Despite the influence of tumor location, it does not appear to be a primary determinant as there was no co-clustering of FD, HGOS, ameloblastoma, giant cell granuloma, and odontogenic myxoma cases in this cluster, which were also (partially) derived from the jaw bones.

Copy number analysis showed that the majority of benign fibro-osseous lesions harbored flat copy number profiles compared with low-grade and HGOSs with chromosomal alterations, which is in line with other publications.[10,20] Interestingly, 1 FD case with *GNAS* mutation and characteristic morphology but unusual course of disease exhibited multiple copy number alterations, including focal gains of the oncogenes *CCND1* and *IGF1R*. This patient was diagnosed with FD at 21 years of age, which manifested as a painful swelling of the skull (frontal and parietal bone) and was managed with debulking. Unusual for FD, the lesion recurred at the same site 19 years later, and caused destruction of the tabula externa frontalis. Biopsy of the lesion showed active monostotic FD, characterized histologically by intervening fibrous stroma containing cytologically bland spindle cells without prominent cytologic atypia (Supplementary Fig. S1). Treatment involved debulking and 8 courses of pamidronate, resulting in stable disease to date without extracranial manifestations. Although FD typically stabilizes upon reaching skeletal maturity, this patient developed FD at an age after skeletal maturation and experienced recurrence 19 years after treatment; the identified copy number alterations may provide an explanation for the unusual course of disease in this particular case. In the literature, rare cases of FD with multiple chromosomal abnormalities have been described, but these were associated with malignant transformation.[34-36]

In this study, we found no copy number changes in COF but identified chromosomal alterations in a few examples of JTOF (2/6) and PsOF (3/19). In PsOF case #3, we detected a gain of chromosome 12 without high-level *MDM2* amplification (Supplementary Fig. S2). Tabareau-Delalande et al[37] observed increased amounts of *MDM2* and *RASAL1* templates in 33% of ossifying fibromas by real-time PCR, particularly in PsOF and JTOF; however, none of these cases showed overexpression of *MDM2* by immunohistochemistry. Recently, Ma et al[10] reported gains of chromosome 12 in 4/29 craniofacial ossifying fibromas, however, it is unclear whether these cases were COF, JTOF, and/or PsOF cases. Bahceci et al[38] reported focal losses in 2/3 PsOF cases but no gains. Further research is required to determine the role of copy number alterations in these subtypes of fibro-osseous tumors of the craniofacial bones and whether these molecular findings are associated with different clinical behavior. Re-evaluation of PsOF case #3 confirmed that the clinical, radiographic, and histomorphologic features were most consistent with PsOF (Supplementary Fig. S2). However, this particular case showed little matrix with a few psammoma bodies compared with the typical morphology observed in the other PsOF cases with numerous psammomatoid bodies, and did not cluster with other PsOF cases. The patient did not develop recurrence or metastasis during 20 years of clinical follow-up.

For future research, we will expand our collection of craniofacial fibro-osseous tumors and histomorphologic mimickers to enhance the diagnostic accuracy of our methylation classifier, as has been demonstrated for brain tumors.[17] It is important to address that DNA methylation classifiers should be used as a complementary diagnostic tool rather than a substitute for expert diagnoses that correlate radiologic and morphologic findings. All classifier predictions must be critically evaluated and correlated

with histologic and clinical information. We consider a comprehensive histologic evaluation essential before proceeding with methylation profiling. Several factors can contribute to incorrect clustering, including low tumor cell content, poor DNA quality, technical issues, and limitations in the reference set's representation of a tumor entity's full spectrum.[17] Furthermore, as demonstrated in this study, tumor location can influence the clustering of individual lesions. Copy number profiling should also be performed in the appropriate clinical context. Many tumor entities exhibit highly recurrent copy number alterations that are diagnostically relevant. For example, *MDM2* amplification is the molecular hallmark of LGOS, depending on the clinical context. On the other hand, polysomy of the long arm of chromosome 12 (comprising *MDM2*) appears to be distinct from typical *MDM2* amplification and can be observed in LGOSs, as shown in this study but has also been reported in ossifying fibromas in the literature. Therefore, this particular finding cannot be used as a specific diagnostic marker.

In conclusion, DNA methylation and copy number profiling can distinguish benign fibro-osseous tumors from low-grade and HGOSs in the craniofacial bones, which is of diagnostic value in challenging cases with overlapping clinicopathological features.

Author Contributions

T.K., B.A., D.B., and A.C. conceived and designed the study; acquired, analyzed, and interpreted the data; and drafted the manuscript. W.S., K.S., A.S., J.B., and A.D. critically revised the manuscript for important intellectual content. W.K., L.K., H.J., I.B., S.M., M.K., M.W., S.P., W.F., T.L., G.B., W.B., J.L., K.L., H.K., M.H., S.K., S.H., M.O., I.E., U.F., L.H., D.S., G.D., and J.D. provided administrative, technical, or material support. D.B. and A.C. supervised this study. All the authors have read and approved the final manuscript.

Data Availability

The data included in the current study are not publicly available but are available from the corresponding author upon reasonable request.

Funding

This study was funded by the International Skeletal Society 2019–2020 Seed Grant. Tony G. Kleijn was supported by a travel grant from the Melanoma and Sarcoma Foundation, Groningen. Baptiste Ameline and Daniel Baumhoer received funding from the Basel Research Centre for Child Health.

Declaration of Competing Interest

The authors declare that they have no conflict of interest.

Ethics Approval and Consent to Participate

The study protocol was approved by the medical ethics committee of the Leiden University Medical Center (B21.022) and University Medical Center Groningen (RR202200287). Research use of tissues and anonymization of data were in accordance with local ethical approvals.

Supplementary Material

The online version contains supplementary material available at https://doi.org/10.1016/j.modpat.2025.100717

References

1. WHO Classification of Tumours Editorial Board. In: *WHO Classification of Head and Neck Tumours. WHO Classification of Tumours*. 5th ed. International Agency for Research on Cancer; 2022.
2. Nelson BL, Phillips BJ. Benign fibro-osseous lesions of the head and neck. *Head Neck Pathol*. 2019;13:466–475. https://doi.org/10.1007/s12105-018-0992-5
3. Cleven AHG, Schreuder WH, Groen E, Kroon HM, Baumhoer D. Molecular findings in maxillofacial bone tumours and its diagnostic value. *Virchows Arch*. 2020;476:159–174. https://doi.org/10.1007/s00428-019-02726-2
4. Kim DY. Current concepts of craniofacial fibrous dysplasia: pathophysiology and treatment. *Arch Craniofac Surg*. 2023;24:41–51. https://doi.org/10.7181/acfs.2023.00101
5. Baumhoer D. Bone-related lesions of the jaws. *Surg Pathol Clin*. 2017;10:693–704. https://doi.org/10.1016/j.path.2017.04.007
6. Lee SE, Lee EH, Park H, et al. The diagnostic utility of the GNAS mutation in patients with fibrous dysplasia: meta-analysis of 168 sporadic cases. *Hum Pathol*. 2012;43:1234–1242. https://doi.org/10.1016/j.humpath.2011.09.012
7. Haefliger S, Turek D, Andrei V, et al. Cemento-osseous dysplasia is caused by RAS-MAPK activation. *Pathology*. 2023;55:324–328. https://doi.org/10.1016/j.pathol.2022.10.006
8. Cleven AHG, Szuhai K, van IJzendoorn DGP, et al. Psammomatoid ossifying fibroma is defined by SATB2 rearrangement. *Mod Pathol*. 2023;36:100013. https://doi.org/10.1016/j.modpat.2022.100013
9. Baumhoer D, Haefliger S, Ameline B, et al. Ossifying fibroma of non-odontogenic origin: a fibro-osseous lesion in the craniofacial skeleton to be (re-) considered. *Head Neck Pathol*. 2022;16:257–267. https://doi.org/10.1007/s12105-021-01351-3
10. Ma M, Liu L, Shi R, et al. Copy number alteration profiling facilitates differential diagnosis between ossifying fibroma and fibrous dysplasia of the jaws. *Int J Oral Sci*. 2021;13:21. https://doi.org/10.1038/s41368-021-00127-3
11. Gomez RS, El Mouatani A, Duarte-Andrade FF, et al. Comprehensive genomic analysis of cemento-ossifying fibroma. *Mod Pathol*. 2024;37:100388. https://doi.org/10.1016/j.modpat.2023.100388
12. Chen Y, Hu DY, Wang TT, et al. CDC73 gene mutations in sporadic ossifying fibroma of the jaws. *Diagn Pathol*. 2016;11:91. https://doi.org/10.1186/s13000-016-0532-0
13. Yoshida A, Ushiku T, Motoi T, et al. Immunohistochemical analysis of MDM2 and CDK4 distinguishes low-grade osteosarcoma from benign mimics. *Mod Pathol*. 2010;23:1279–1288. https://doi.org/10.1038/modpathol.2010.124
14. Bahceci DH, Jordan RCK, Horvai AE. MDM2 gene amplification and expression of MDM2 and CDK4 are rare in ossifying fibroma of craniofacial bones. *Head Neck Pathol*. 2022;16:991–997. https://doi.org/10.1007/s12105-022-01454-5
15. Kansara M, Teng MW, Smyth MJ, Thomas DM. Translational biology of osteosarcoma. *Nat Rev Cancer*. 2014;14:722–735. https://doi.org/10.1038/nrc3838
16. Papanicolau-Sengos A, Aldape K. DNA methylation profiling: an emerging paradigm for cancer diagnosis. *Annu Rev Pathol*. 2022;17:295–321. https://doi.org/10.1146/annurev-pathol-042220-022304
17. Koelsche C, von Deimling A. Methylation classifiers: brain tumors, sarcomas, and what's next. *Genes Chromosomes Cancer*. 2022;61:346–355. https://doi.org/10.1002/gcc.23041
18. Koelsche C, Schrimpf D, Stichel D, et al. Sarcoma classification by DNA methylation profiling. *Nat Commun*. 2021;12:498. https://doi.org/10.1038/s41467-020-20603-4
19. Lyskjaer I, De Noon S, Tirabosco R, et al. DNA methylation-based profiling of bone and soft tissue tumours: a validation study of the "DKFZ sarcoma classifier.". *J Pathol Clin Res*. 2021;7:350–360. https://doi.org/10.1002/cjp2.215
20. Ameline B, Nathrath M, Nord KH, et al. Methylation and copy number profiling: emerging tools to differentiate osteoblastoma from malignant mimics? *Mod Pathol*. 2022;35:1204–1211. https://doi.org/10.1038/s41379-022-01071-1
21. Pongpanich M, Sanguansin S, Kengkarn S, Chaiwongkot A, Klongnoi B, Kitkumthorn N. An integrative analysis of genome-wide methylation and expression in ameloblastoma: a pilot study. *Oral Dis*. 2021;27:1455–1467. https://doi.org/10.1111/odi.13666
22. Guimarães LM, Baumhoer D, Andrei V, et al. DNA methylation profile discriminates sporadic giant cell granulomas of the jaws and cherubism from their giant cell-rich histological mimics. *J Pathol Clin Res*. 2023;9:464–474. https://doi.org/10.1002/cjp2.337
23. Worst BC, van Tilburg CM, Balasubramanian GP, et al. Next-generation personalised medicine for high-risk paediatric cancer patients – the INFORM pilot study. *Eur J Cancer*. 2016;65:91–101. https://doi.org/10.1016/j.ejca.2016.06.009

24. Pires SF, de Barros JS, da Costa SS, et al. DNA methylation patterns suggest the involvement of DNMT3B and TET1 in osteosarcoma development. *Mol Genet Genomics*. 2023;298:721−733. https://doi.org/10.1007/s00438-023-02010-8
25. Barenboim M, Kovac M, Ameline B, et al. DNA methylation-based classifier and gene expression signatures detect BRCAness in osteosarcoma. *PLoS Comput Biol*. 2021;17:e1009562. https://doi.org/10.1371/journal.pcbi.1009562
26. Giesche J, Mellert K, Geißler S, et al. Epigenetic lockdown of CDKN1A (p21) and CDKN2A (p16) characterises the neoplastic spindle cell component of giant cell tumours of bone. *J Pathol*. 2022;257:687−696. https://doi.org/10.1002/path.5925
27. Kleijn TG, Ameline B, Schreuder WH, et al. Odontogenic myxomas harbor recurrent copy number alterations and a distinct methylation signature. *Am J Surg Pathol*. 2024;48:1224−1232. https://doi.org/10.1097/PAS.0000000000002293
28. Daenekas B, Pérez E, Boniolo F, et al. Conumee 2.0: enhanced copy-number variation analysis from DNA methylation arrays for humans and mice. *Bioinformatics*. 2024;40:btae029. https://doi.org/10.1093/bioinformatics/btae029
29. Miettinen M, Abdullaev Z, Turakulov R, et al. Assessment of the utility of the sarcoma DNA methylation classifier in surgical pathology. *Am J Surg Pathol*. 2024;48:112−122. https://doi.org/10.1097/PAS.0000000000002138
30. Roohani S, Ehret F, Perez E, et al. Sarcoma classification by DNA methylation profiling in clinical everyday life: the Charité experience. *Clin Epigenetics*. 2022;14:149. https://doi.org/10.1186/s13148-022-01365-w
31. Baumhoer D, Hench J, Amary F. Recent advances in molecular profiling of bone and soft tissue tumors. *Skeletal Radiol*. 2024;53:1925−1936. https://doi.org/10.1007/s00256-024-04584-9
32. Weber M, Wehrhan F, Deschner J, et al. The special developmental biology of craniofacial tissues enables the understanding of oral and maxillofacial physiology and diseases. *Int J Mol Sci*. 2021;22:1315. https://doi.org/10.3390/ijms22031315
33. Jurmeister P, Wrede N, Hoffmann I, et al. Mucosal melanomas of different anatomic sites share a common global DNA methylation profile with cutaneous melanoma but show location-dependent patterns of genetic and epigenetic alterations. *J Pathol*. 2022;256:61−70. https://doi.org/10.1002/path.5808
34. Shi R, Li X, Zhang J, et al. Clinicopathological and genetic study of a rare occurrence: malignant transformation of fibrous dysplasia of the jaws. *Mol Genet Genomic Med*. 2022;10:e1861. https://doi.org/10.1002/mgg3.1861
35. Jhala DN, Eltoum I, Carroll AJ, et al. Osteosarcoma in a patient with McCune−Albright syndrome and Mazabraud's syndrome: a case report emphasizing the cytological and cytogenetic findings. *Hum Pathol*. 2003;34:1354−1357. https://doi.org/10.1016/j.humpath.2003.08.004
36. Hatano H, Morita T, Ariizumi T, Kawashima H, Ogose A. Malignant transformation of fibrous dysplasia: a case report. *Oncol Lett*. 2014;8:384−386. https://doi.org/10.3892/ol.2014.2082
37. Tabareau-Delalande F, Collin C, Gomez-Brouchet A, et al. Chromosome 12 long arm rearrangement covering MDM2 and RASAL1 is associated with aggressive craniofacial juvenile ossifying fibroma and extracranial psammomatoid fibro-osseous lesions. *Mod Pathol*. 2015;28:48−56. https://doi.org/10.1038/modpathol.2014.80
38. Bahceci DH, Grenert JP, Jordan RCK, Horvai AE. Genomic profiling of the craniofacial ossifying fibroma by next-generation sequencing. *Head Neck Pathol*. 2023;17:722−730. https://doi.org/10.1007/s12105-022-01523-9